ADVANCED MATERIALS TECHNOLOGIES
www.advmattechnol.de

Check for updates

Metal Coated Conductive Fabrics with Graphite Electrodes and Biocompatible Gel Electrolyte for Wearable Supercapacitors

*Abhilash Pullanchiyodan, Libu Manjakkal, Saoirse Dervin, Dhayalan Shakthivel, and Ravinder Dahiya**

Fabric-based supercapacitors have received considerable interest as energy storage devices for wearable systems. This work demonstrates the use of metal coated fabrics as the active material and current collector with nontoxic polyvinyl alcohol (PVA)-KCl gel electrolyte for wearable supercapacitors (SCs). To evaluate the influence of the metal coating, the electrochemical and capacitive studies are carried out and results are compared with a newly developed metal free graphite printed textile (cellulose-polyester) (CP-Gr) based SC. It is evident that the homemade graphite paste electrode printed on the top of Armor FR (Ni/Cu coated polyester fabric) (AFR-Gr) and Nora Dell (Ni/Cu/Ag coated polyamide) (ND-Gr) based SCs with PVA-KCl electrolyte exhibits the specific capacitance of 99.06 and 46.88 mF cm^{-2}, respectively, at sweep rate of 5 mV s^{-1}. These values are 24 and 52 times greater than that of CP-Gr based SC. The AFR-Gr and ND-Gr based SCs have an excellent energy density of 8.81 and 4.17 μWh cm^{-2}, respectively, at 5 mV s^{-1}. The fabricated ND-Gr based SC gives a stable response for more than 5000 charging/discharging cycles. Finally, the nontoxic nature of the PVA-KCl gel electrolyte is evaluated and confirmed through in vitro cytocompatibility assessment with adult human dermal fibroblasts cells for wearable applications.

1. Introduction

Wearable energy storage devices are needed in diverse smart systems and their applications in electronic skin (eSkin), sportswear, healthcare, robotics, etc.[1] The fabric-based supercapacitors (FSCs) are considered suitable for such applications due to attractive features such as light weight, flexibility, ease of integration, and portability.[2,3] Further, they can be seamlessly integrated on textiles by stitching or weaving.[1c,3,4] The high porosity of textile as substrate is also a major attraction for these supercapacitor (SC)[5] as they offer greater adsorption capability of the active materials.[6] Despite these advantages, the widespread use of FSCs is still elusive, owing to the issues such as inefficient current collectors, lack of high performing electrode materials, and safe electrolytes.[6]

Most of the reported FSCs use either metal sheets or carbon coated cloth as the current collector,[7] even if there are clear demerits. For example, the thin metal films adversely affect the flexibility of SCs and increase the total weight. Further, most of the previously reported works on metal coated fabric SCs have used toxic, acidic, or alkaline electrolytes,[8] which affect the acceptance of wearable systems. For example, the metal oxides based active electrode are highly unstable in acidic electrolyte used in SCs.[9] Likewise, the other alternative, i.e., carbon cloth based current collectors suffer from poor power density, low electrical conductivity (≈10^2 S m^{-1}), and poor mechanical strength, even if they exhibit good capacitance.[6,10] The poor scalability, cost, and controllability are some other drawbacks of carbonized cotton fabrics, which is one of the widely used carbon cloth as current collector in textile-based SCs.[6] The solutions to the above challenges could come from lightweight materials such as textiles coated with metal nanoparticle.[6,11] Recently, a textile SC developed on a Ni/Cu/Ni/Au layers deposited polyester woven textile with ZnO nanowire and nickel hydroxide as the active electrode material shows a specific capacitance of 3150 F g^{-1} in a 1 M LiOH aqueous solution.[12] Similarly, Li et al. showed an enhancement in performance of textile-based carbon-nanotube (CNT) SC through the introduction of metal (Cu and Au) coated polyethylene terephthalate (PET) fabrics as a current collector.[13] The results offered almost 60 times enhancement in performance for CNT/Cu/PET and CNT/Au/PET based SC compared to CNT/PET fabric.[13] However, currently the low life cycle and reduced performance due to redox reactions are the major issues with metal nanoparticle for electrodes in SCs.

Herein we use carbon-based materials deposited on metal coated fabric to demonstrate the solution to above issues. We have investigated the electrochemical performance of four types (i.e., i) Berlin RS, ii) Bremen RS, iii) Nora Dell (ND),

Dr. A. Pullanchiyodan, Dr. L. Manjakkal, S. Dervin, Dr. D. Shakthivel, Prof. R. Dahiya
Bendable Electronics and Sensing Technologies (BEST) Group
School of Engineering
University of Glasgow
Glasgow G12 8QQ, UK
E-mail: Ravinder.Dahiya@glasgow.ac.uk

The ORCID identification number(s) for the author(s) of this article can be found under https://doi.org/10.1002/admt.201901107.

© 2020 The Authors. Published by WILEY-VCH Verlag GmbH & Co. KGaA, Weinheim. This is an open access article under the terms of the Creative Commons Attribution License, which permits use, distribution and reproduction in any medium, provided the original work is properly cited.

DOI: 10.1002/admt.201901107

 © 2020 The Authors. Published by WILEY-VCH Verlag GmbH & Co. KGaA, Weinheim

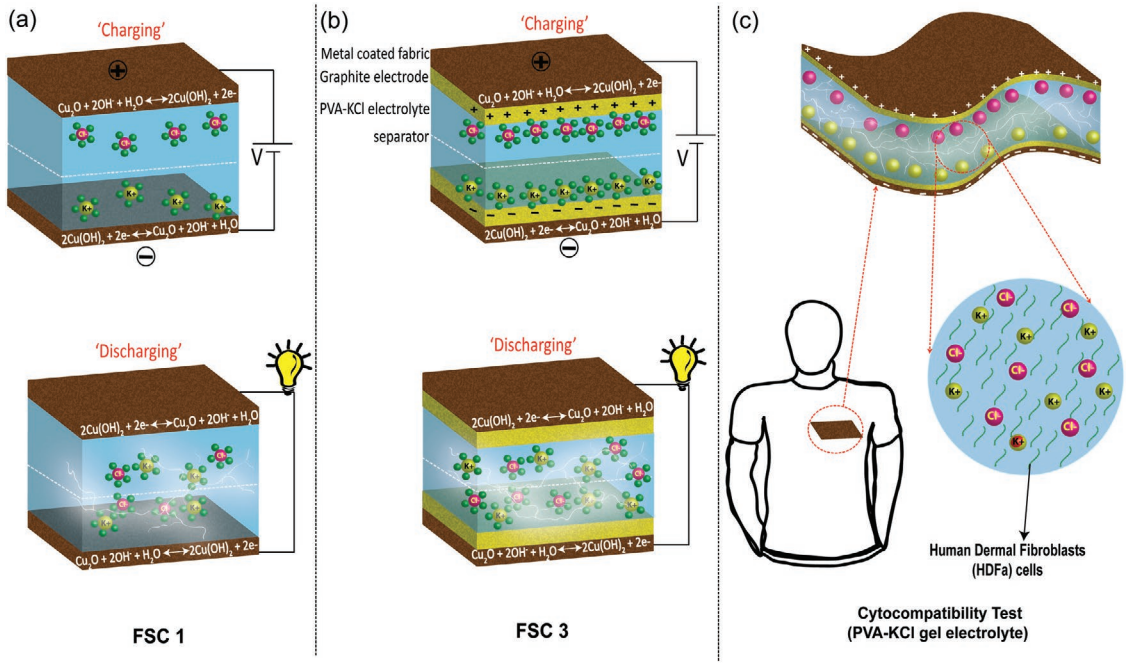

Figure 1. a,b) Schematic diagram showing the charging and discharging mechanism of FSC 1 and FSC 3, respectively, and c) the biocompatibility assessment of the nontoxic PVA-KCl gel electrolyte.

and iv) Armor FR, AFR) of metal coated commercial fabrics as electrode and current collector. A schematic diagram showing the charging and discharging mechanism of this metal coated fabric SC (FSC 1) is shown in **Figure 1**a. Further, an in-house formulated graphite paste was printed on the top of the metal coated cloth to improve the performance of the FSCs (Figure 1b). For example, in the case of Armor FR based cloth with graphite paste on it, the specific capacitance of SC at 5 mV s^{-1} increased from 50 to 99.06 mF cm^{-2} (1.4 F g^{-1}) as compared to the cloth without the graphite paste. The role of the graphite paste toward performance improvement was investigated. Further, we have used nontoxic polyvinyl alcohol (PVA)-KCl gel electrolyte, which is generally used to prevent electrolyte leakage in textile SCs. Due to user safety concerns, the use of nontoxic materials is desired in wearable systems.[14] For example, the leakage of acidic or alkaline electrolytes may result in skin rashes. In this regard, the KCl based neutral electrolytes (e.g., PVA-KCl) are attractive as they offer high ionic conductivity and smaller hydration sphere.[9] However, the biocompatibility of such gel electrolytes has not been evaluated. In this work, we also report a method to test the biocompatibility of the PVA-KCl gel electrolyte (Figure 1c). The cytocompatibility assessment showed excellent adhesion and proliferation of human dermal fibroblasts, adult (HDFa) cells on the electrolyte surface, confirming the nontoxic nature of PVA-KCl gel electrolyte. Subsequently, we also analyzed and compared the influence of different types of gel electrolytes, including neutral (KCl), basic (NaOH), and acidic (H_3PO_4) on the electrochemical performance of graphite printed metal coated FSCs. The performance of the developed SCs along with electrolyte biocompatibility is compared with state of the art, and the results are summarized in **Table 1**.[8b,c,11a,12,15]

2. Results and Discussion

2.1. Performance of Metal Coated Fabric Supercapacitor (FSC 1)

In the present study, four metal plated conducting fabrics such as Berlin RS, Bremen RS, Nora Dell, and Armor FR were tested for electrode as well as current collector applications. Herein, Berlin RS (silk, polyamide) and Bremen RS (Parachute silk, polyamide) are silk based textile coated with silver. Nora Dell is a polyamide-based fabric having Ni/Cu/Ag as the conductive coating, whereas, Armor FR is a polyester woven fabric having Ni/Cu as the conducting metals. Table S1 in the Supporting Information gives more specifications of these fabrics. The photographs of all the four-metal deposited conducting fabrics along with the graphite coated Armor FR (AFR-Gr) and Nora dell (ND-Gr) are given in **Figure 2**a. Figure 2b shows the prototype of the fabricated flexible AFR-Gr based SC. The electrochemical properties of the metal coated symmetric FSCs were tested by cyclic voltammetry (CV) using 0.1 M aqueous KCl electrolyte. Figure 2d shows the CV curve of the electrodes at a scan rate of 100 mV s^{-1}, with all four conducting fabric based SCs showing a distorted rectangular CV curve. For a constant scan rate, the Armor FR and Nora Dell based SCs exhibited much wider area under the CV curve than the Berlin and Bremen based SCs. The areal capacitances (C_A) of these SCs were obtained from the area under the CV curve by using Equation (4) given in the Experimental Section. The value of C_A from individual CV curves is shown in Figure S1 in the Supporting Information. The comparison of C_A at a scan rate of 100 mV s^{-1}, shown in Figure 2e, clearly indicates that the Armor FR based FSC has the highest C_A (≈90 mF cm^{-2}). The C_A of Nora Dell (20.6 mF cm^{-2}), Bremen RS (3.28 mF cm^{-2}), and Berlin RS (5.15 mF cm^{-2}) are much lower. The electrochemical impedance spectroscopic (EIS) analysis was also carried out to investigate the

© 2020 The Authors. Published by WILEY-VCH Verlag GmbH & Co. KGaA, Weinheim

Table 1. Comparison of the performance of metal coated FSC with state of the art.

Fabric[a)]	Electrode material	Electrolyte	Biocompatibility (electrolyte)	Specific capacitance	Energy density	Power density	Ref.
Ni/Cu/Ni/Au coated polyester	$Ni(OH)_2$ on ZnO NW	1 M LiOH	Not mentioned	3150 F g^{-1}	54 W h kg^{-1}	110 kW kg^{-1}	[12]
Au-coated textile fiber	ZnO NF/NiCo LDH	1 M LiOH	Not mentioned	1624 F g^{-1}	48.32 W h kg^{-1}	27.53 kW kg^{-1}	[15]
Ni/Cu/Ni/Au coated polyester	V_2O_5 (3 nm) coated graphene/MWCNT	2 M KCl	Not mentioned	2590 F g^{-1} (1 mV s^{-1})	96 W h kg^{-1}	800 W kg^{-1}	[8b]
Cu-coated PET fibers	β-$Co(OH)_2$	1 M KOH	Not mentioned	108.7 F g^{-1} (three electrode)	–	–	[8c]
Cu coated PET	CNT	PVA/H_3PO_4	Not mentioned	4.312 mF cm^{-2}	8.517 μW h cm^{-3}	≈1 mW cm^{-3}	[11]
Au coated PET	CNT	PVA/H_3PO_4	Not mentioned	3.683 mF cm^{-2}	8.183 μW h cm^{-3}	≈1 mW cm^{-3}	[11]
Armor FR	$Cu_2O/Cu(OH)_2$	PVA/KCl	Biocompatible	50.0 mF cm^{-2} (5 mV s^{-1})	1.74 μW h cm^{-2}	9.5 mW cm^{-2}	This work
Armor FR	$Cu_2O/Cu(OH)_2$/ graphite paste	PVA/KCl	Biocompatible	99.06 mF cm^{-2} (5 mV s^{-1})	8.81 μW h cm^{-2}	20.0 mW cm^{-2}	This work

[a)]NW: nanowire, NF: nanoflower, PET: polyethylene terephthalate fabrics, LDH: layered double hydroxide.

ion/electron transport behavior, ionic or charge transfer resistance, and the capacitive behavior of the metal coated SC electrodes.[16] The Nyquist plots of all four-metal coated conducting fabrics in 0.1 M KCl aqueous electrolyte, shown in Figure 2c, show that the Armor FR has an equivalent series resistance (ESR) of around 9.3 Ω, whereas Nora Dell exhibits 5.3 Ω. In this Nyquist plot, mainly the high frequency domain contributed to the electrode resistance and this is followed by electrolyte resistance. On other hand, the low frequency domain is responsible for the diffusion layer resistance and capacitive behavior of the material.[17] To understand the capacitance mechanism, the slope of the Nyquist curves (Figure 2c) was analyzed in the low frequency region. The low values of slopes (0.82 for Nora Dell, 0.74 for Berlin RS, 0.58 for Bremen RS, and 0.53 for Armor FR) suggest that the device charging is limited by ion diffusion from the electrolyte.[17] All the four Nyquist plots were fitted by equivalent circuit (details are provided in the Supporting Information) using multiple EIS parameterization software[18] and the results were explained in Figure S2

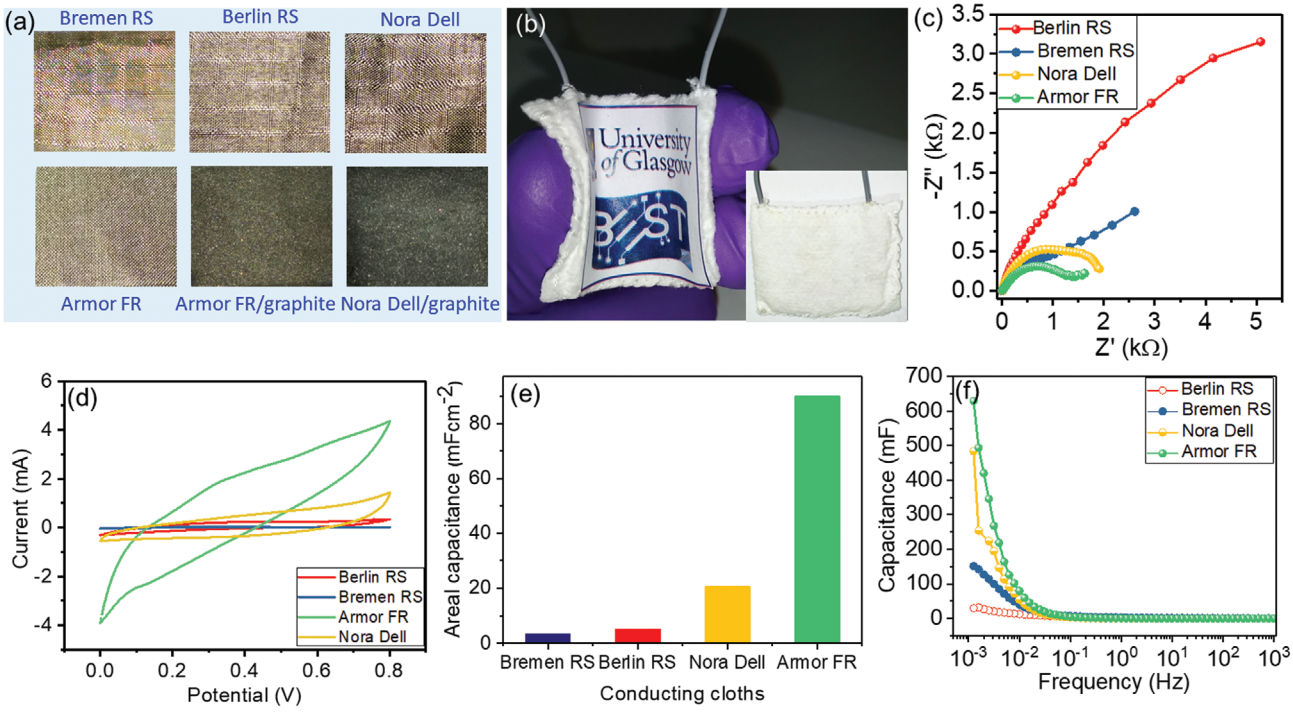

Figure 2. a) Image of the metal coated and graphite pasted fabric electrodes used for SC fabrication, b) photograph of the fabricated FSC (AFR-Gr), c) Nyquist plot, d) CV curve (scan rate-100 mV s^{-1}), e) areal capacitance (scan rate of 1 mV s^{-1}), and f) variation of capacitance with frequency of various conducting fabrics based SC in 0.1 M KCl electrolyte.

© 2020 The Authors. Published by WILEY-VCH Verlag GmbH & Co. KGaA, Weinheim

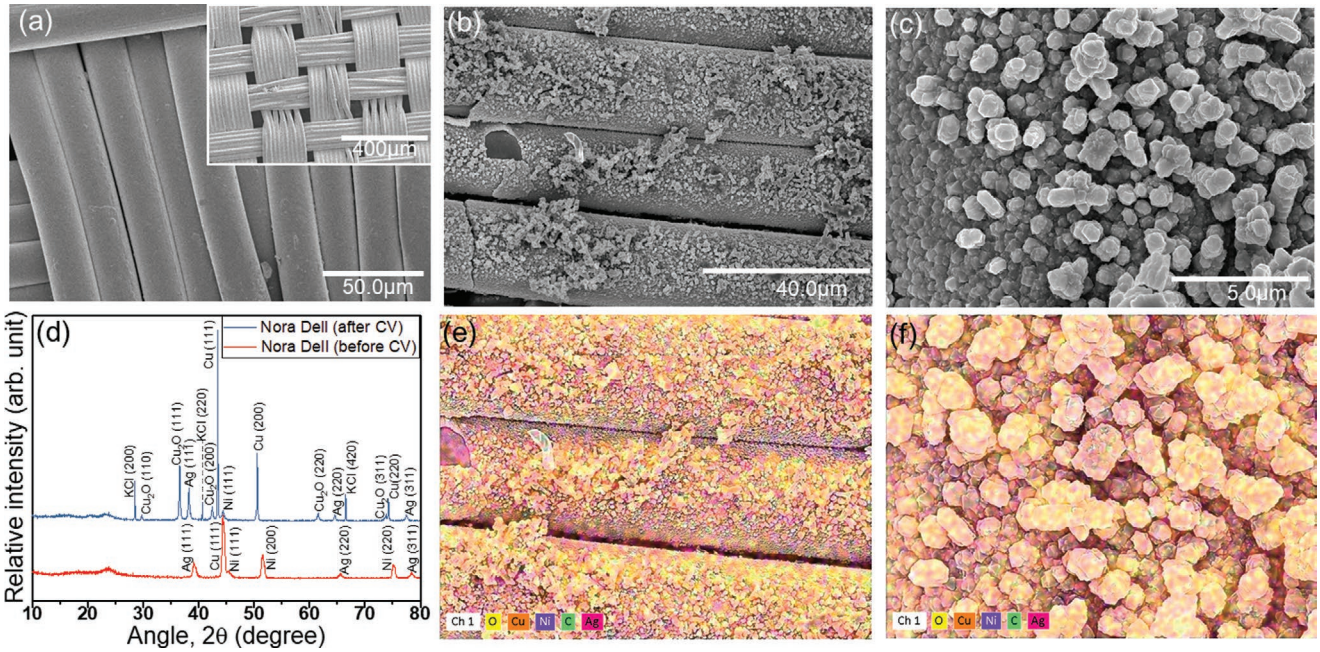

Figure 3. a) SEM image of bare Nora Dell fabric (inset: low resolution image) before CV, b,c) SEM images of Nora Dell fabric after CV, d) XRD pattern of Nora Dell (before and after CV), and e,f) EDX mapping of Nora Dell (after CV).

and Table S3 in the Supporting Information. The capacitance of the SCs at different frequencies is shown in Figure 2f. The Armor FR based device clearly shows the highest capacitance. With electrochemical analysis evidently showing that Armor FR and Nora Dell have excellent electrochemical properties for SCs, their suitability for FSCs was further investigated.

The high value of capacitance for Armor FR and Nora Dell is attributed to the redox reaction taking place in Ni and Cu metal (present in the fabric) during the electrochemical process. To confirm this, we carried out a detailed microstructural and morphological analysis of the Nora Dell and Armor FR fabric before and after CV measurements. **Figure 3**a–c represents the microstructural and morphological analysis of the Nora Dell before and after CV measurement. A similar result for the Armor FR is discussed in Figure S3 in the Supporting Information. Figure 3a, shows the scanning electron microscopic (SEM) image of bare Nora Dell fabric prior to the electrochemical reaction. The inset in the Figure 3a shows the low-magnification image of the same. A uniform defect free metal coating on the fabric is evident from Figure 3a. During CV measurement the metal, present on the surface of fabric, undergoes redox reaction within the electrolyte and consequently gets converted into nanostructured metal oxides and hydroxides as per Equations (1)–(3).[19]

$$2Cu + H_2O \rightarrow Cu_2O + 2H^+ + 2e^- \quad (1)$$

$$Cu_2O + 2OH^- + H_2O \leftrightarrow 2Cu(OH)_2 + 2e^- \quad (2)$$

$$NiO + OH^- \leftrightarrow NiOOH + e^- \quad (3)$$

This is clearly visible from the microstructure on the fabric after CV (Figure 3b,c). In order to understand the composition of these nanomaterials, the energy dispersive X-ray spectroscopic (EDX) analysis was carried out. The EDX mapping (Figure 3e,f) results confirm that the metal underwent oxidation after reacting with electrolyte (Equation (1)) and the major phase formed in this process is copper oxide. This is also confirmed by the X-ray diffractometer (XRD) analysis presented in Figure 3d. The XRD pattern of the bare fabric (before CV) clearly shows the presence of Cu, Ni, and Ag metal on the textiles and all the peak positions are indexed using standard International Centre for Diffraction Data (ICDD) patterns (Cu: 71-4610; Ag: 71-4612, 72-6549; Ni: 71-4653, 88-2326). The slight broadening of peaks suggests that coated metal particles are preferably in nanometer range. However, during the CV, the Cu undergoes an oxidation and forms Cu_2O as evident from the XRD pattern of the Nora Dell fabric (after CV). All peaks corresponding to Cu_2O could be indexed using standard ICDD file (73-6371). From the well-defined peaks it is also evident that the grain growth occurs during the redox reaction and large sized particles are formed. The size and shape of the formed Cu_2O particles depend on several factors such as applied potential, diffusion rate of ions, amount of Cl^- ions in the solution, and degree of branch chain formation of Cu_2O.[19a] Apart from the Cu_2O, the peaks corresponding to KCl (ICDD: 75-0296) are also observed. This could be due to the crystallization of KCl salt on the fabric from the electrolyte solution (after drying). The peaks corresponding to pure Cu, Ni, and Ag are also present in the fabric. This suggests that Cu is more prone to oxidation and it undergoes partial oxidation during the initial cycles. It is well known that the surface area of the electrode material plays a significant role in electrical double layer capacitance (EDLC) as it can adsorb more ions and hence increases the capacitance. Consequently, the nanoparticle like morphology of the resulting oxides increases the active material surface area, which in turn enhances the capacitance of the FSC. The Armor FR based fabric also demonstrates similar behavior. It is also noted that after the electrochemical

© 2020 The Authors. Published by WILEY-VCH Verlag GmbH & Co. KGaA, Weinheim

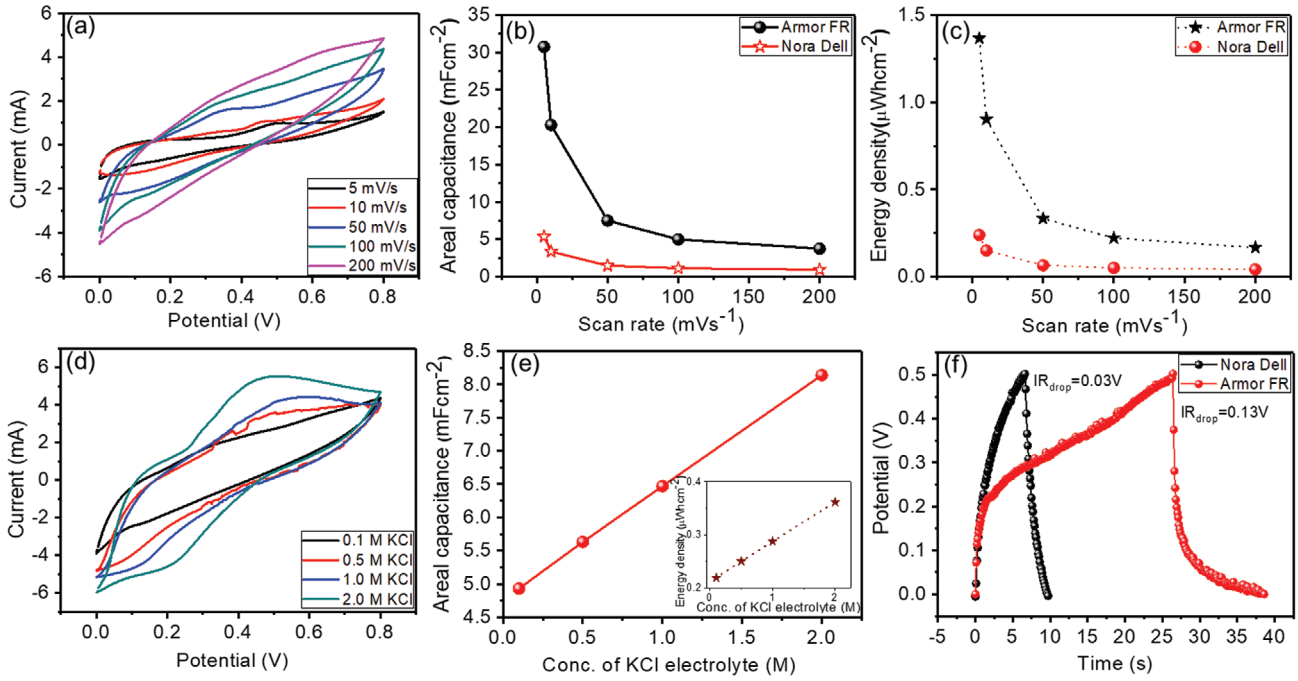

Figure 4. a) CV curves of Armor FR based SC in 0.1 M KCl electrolyte and b,c) variation of areal capacitance and energy density of Armor FR and Nora Dell based SC, respectively, with different scan rates, d) CV curves of Armor FR based SC with different KCl concentrations, e) variation of areal capacitance with KCl concentration (inset variation of energy density), and f) GCD plot of Armor FR and Nora Dell based SC in 0.1 M KCl electrolyte.

reaction the copper found in the Armor FR based SC gets oxidized to form Cu_2O and $Cu(OH)_2$, which is having high C_A (see Figure S3, Supporting Information). This is presumably the reason for the high capacitance achieved in the Armor FR based SC in comparison to the other FSCs.

Figure 4a shows the CV curves of Armor FR with different scan rates (5–200 mV s^{-1}). The CV curves of Nora Dell are shown in Figure S4a in the Supporting Information. The Armor FR CV shows a quasi-rectangular behavior especially at higher scan rates. At the low scan rates, the CV curves clearly indicate a small peak (around 0.5 V in 5 mV s^{-1} scan rate) and its value slightly decreases as the scan rate increases. This is presumably due to the oxidation of Cu (Figure S4b,c, Supporting Information), which is also evidenced by the XRD spectra. In the case of Nora Dell (Figure S4, Supporting Information) the CV curve shows a quasi-rectangular shape, with the redox peak observed at very low scan rate (1 mV s^{-1}) for a potential of 0.3 V. The C_A of both electrodes with different scan rates is presented in Figure 4b. The Armor FR has higher C_A value as compared to that of Nora Dell. As with several textile-based SCs reported previously,[4a,8c,20] the C_A value decreases with increase in the scan rate.

The energy densities of Armor FR and Nora Dell based SCs were measured from CV analysis (Equation (5) in the Experimental Section). The observed energy densities of the Armor FR and Nora Dell based metal coated SCs are shown in Figure 4c. From these results, it may be observed that at a CV scan rate of 5 mV s^{-1} the energy density of Armor FR (≈1.35 μWh. cm^{-2}) without gel electrolyte is almost six times higher than that of Nora Dell (0.24 μWh. cm^{-2}). In order to understand the effect of electrolyte concentration on the performance of the textile materials, we conducted electrochemical studies with varying concentrations of KCl (from 0.1 to 2.0 M). Figure 4d shows the CV curves of Armor FR fabric at scan rate of 100 mV s^{-1} with varying electrolyte concentration. From Figure 4d it is evident that the peak current increases with increase in electrolyte concentration. The same trend is also observed for C_A (Figure 4e) and energy density (inset of Figure 4e) with various concentrations of KCl. A maximum energy density and C_A for the Armor FR textiles SC are achieved with 2.0 M KCl. It is also noted that with increase in KCl concentration the ESR value decreases from 9.3 Ω for 0.1 M KCl to 2.0 Ω for 2.0 M KCl electrolyte. A similar observation found for Nora Dell based SC is discussed in Figure S5 in the Supporting Information. For a clearer interpretation of the influence of cation (K^+) concentration on capacitance, we plotted the variation of C_A with pK of KCl (–log [K^+]) electrolyte solution and the results are given in Figure S5 in the Supporting Information. It is clear from the figure that for Armor FR, the C_A value increases with increase in the K^+ ion concentration. At the same time, the maximum capacitance of the Nora Dell textiles was achieved at an electrolyte concentration of 1.0 M KCl, and thereafter the value decreases slightly, presumably due to saturation of K^+ ion adsorption on the surface of the textile.

The SC performance of the devices was further investigated using galvanostatic charging–discharging (GCD) analysis. These GCD measurements were investigated in a potential of 0.5 V with an applied current of 0.5 mA and the results are given in Figure 4f. From the results it can be noticed that the Nora Dell based device shows better GCD cycle with a very low potential drop (IR_{drop} = 0.03 V), compared to Armor FR (IR_{drop} = 0.13 V). The Nora Dell based device also shows good

© 2020 The Authors. Published by WILEY-VCH Verlag GmbH & Co. KGaA, Weinheim

cyclic stability of almost 3000 cycles (discussed in Figure S5, Supporting Information). The high IR_{drop} in Armor FR compared to Nora Dell is due to the nonreversible electrochemical reaction between the Cu and the electrolyte, which leads to decrease in electrical conductivity and the loss of contact with current collector.[8c] On the other hand, due to presence of silver, the Nora Dell based SC retains its conductivity to an extent and results in a lower potential drift in GCD cycles.

In order to maintain the flexibility and to avoid complicated packaging or leakage of the electrolyte, we also analyzed the electrochemical properties of Nora Dell and Armor FR fabrics with PVA-KCl gel electrolyte. A detailed CV and EIS analysis of these FSCs in gel electrolyte is discussed in Figure S6 in the Supporting Information. We observed that the Armor FR based SC exhibits a C_A of 50 mF cm^{-2} at a scan rate of 5 mV s^{-1}, which is almost four times higher than that of Nora Dell based SC (12 mF cm^{-2}) in PVA-KCl gel electrolyte. Similarly, for Armor FR fabric the measured energy density is higher than that of Nora Dell based SC. However, the power density of Nora Dell (obtained by Equation (6) given in the Experimental Section) is significantly higher than that of Armor FR. This is due to high ESR value (1.64 Ω) for Armor FR than Nora Dell (0.38 Ω), which was obtained by EIS analysis. The low ESR value for Nora Dell based SC is due to the presence of high conducting silver in the fabric. On other hand, Armor FR has only Cu/Ni. It is also evident from the XRD analysis that silver is less prone to oxidation during the electrochemical reaction, which obviously maintains the electrical conductivity of the fabric. On the other hand, Ni and Cu present in both fabrics (Armor FR and Nora Dell) get oxidized during the electrochemical reaction and result in increased ESR. The GCD analysis of the SC in gel electrolyte was also investigated. The typical GCD curves of Nora Dell-PVA-KCl gel electrolyte-based SC at different applied current (0.6–1.0 mA) are given in Figure S6 in the Supporting Information. The device shows an IR_{drop} of 0.02 V at an applied current of 0.6 mA, which is comparable with the result obtained from the device based on aqueous KCl electrolyte (0.03 V).

2.2. Electrochemical Analysis of Graphite Printed Textiles (Both Bare and Metal Coated Cloth) in PVA-KCl Gel Electrolyte

To further enhance the performance of the conducting FSCs the textiles were coated with inhouse formulated graphite paste (Figure 1b). Graphite was chosen here to develop the paste because carbon based materials are conductive, and stable in different electrolyte.[21] Further, they are cost effective and eco-friendly. The viscosity analysis of the formulated paste was given in Figure S7 in the Supporting Information. In order to compare the role of metal particles (present on the commercially sourced fabrics) on SC performance we also fabricated a textile SC on bare (metal-free) cellulose/polyester blend fabric by printing the graphite paste as both current collector and active electrode material. **Figure 5**a shows the Nyquist plots of AFR-Gr, ND-Gr, and cellulose/polyester-graphite (CP-Gr) FSCs, respectively. The corresponding Bode plots are given in Figure 5b. It is evident from Figure 5a that CP-Gr shows high impedance value with an ESR of 238 Ω compared to AFR-Gr (2 Ω) and ND-Gr (1 Ω). This high ESR value and charge transfer resistance in CP-Gr are due

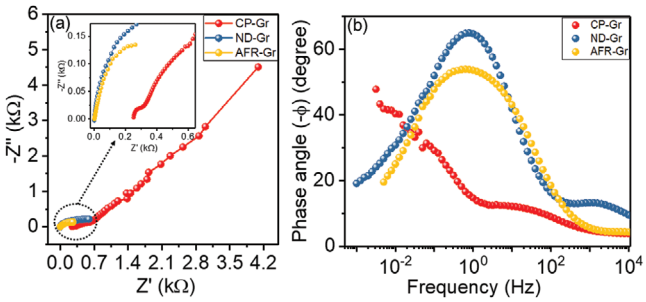

Figure 5. a) Nyquist plots (inset zoomed area) and b) Bode plots of AFR-Gr, ND-Gr, and CP-Gr based SCs.

to the high electrolytic and contact resistance between the current collector and active material.[22] This is directly attributed to the less conductive graphite printed current collector (CP-Gr), compared to metal coated fabric in AFR-Gr and ND-Gr. In the low frequency domain, the CP-Gr device shows a straight-line nature, indicating the capacitive nature of graphite electrode. The phase angle of each device is measured from the Bode plots. The CP-Gr device shows a phase angle of 45°, whereas AFR-Gr and ND-Gr have 55° and 65°, respectively. These values suggest the capacitive nature of the electrode material. The corresponding CV results of all these FSCs are given in **Figure 6**a–c for AFR-Gr, ND-Gr, and CP-Gr, respectively. As evident from Figure 6c, the electrode does not undergo any Faradic reactions in the case of CP-Gr device. Whereas for AFR-Gr and ND-Gr based devices the typical redox reaction peaks are clearly visible in the CV curve (Figure 6a,b). These results indicate that in addition to the graphite's EDLC, the redox reaction in metal particles on fabric (mostly in Cu and Ni) also contribute to the total capacitance. Hence, this Faradic process and the EDLC formation in the graphite synergistically contribute to the enhancement of the capacitance of device. The AFR-Gr and ND-Gr based SC device shows a specific capacitance of 99 mF cm^{-2} (1.4 F g^{-1}) and 47 mF cm^{-2} (896 mF g^{-1}), respectively. These values are higher than that of CP-Gr based SC (1.89 mF cm^{-2}) and graphite uncoated metal coated fabric (50 mF cm^{-2} for Armor FR and 11.91 mF cm^{-2} for Nora Dell). The energy density and power density of each of these devices are calculated and the results are discussed in the next section. XRD patterns and SEM images of the graphite printed on AFR-Gr and ND-Gr were shown in Figure S7 in the Supporting Information. The porous nature of graphite electrode was clear from the images and the corresponding peaks for graphite were indexed in the XRD pattern.

The GCD analysis of ND-Gr based SC device in Figure 6d shows the variation of GCD with different applied currents ranging from 1.0 to 2.0 mA. The device shows an IR_{drop} of 0.03 V at an applied current of 1.0 mA. The stability of the developed device is analyzed up to 5000 GCD cycles. Figure 6e,f shows the first and last 25 cycles of 5000 GCD cycles. No device breakage suggests that it will continue to perform after 5000 cycles. However, the capacitance retention of the device is comparatively less (around 60% after 5000 cycles). This may be due to the nonreversible interaction of Cu with KCl electrolyte during the charging–discharging process[8c] and due to the insertion/deinsertion of larger K^+ ions that eventually lead to the electrode rupture and contact loss with current collector.[23] Similarly, the

© 2020 The Authors. Published by WILEY-VCH Verlag GmbH & Co. KGaA, Weinheim

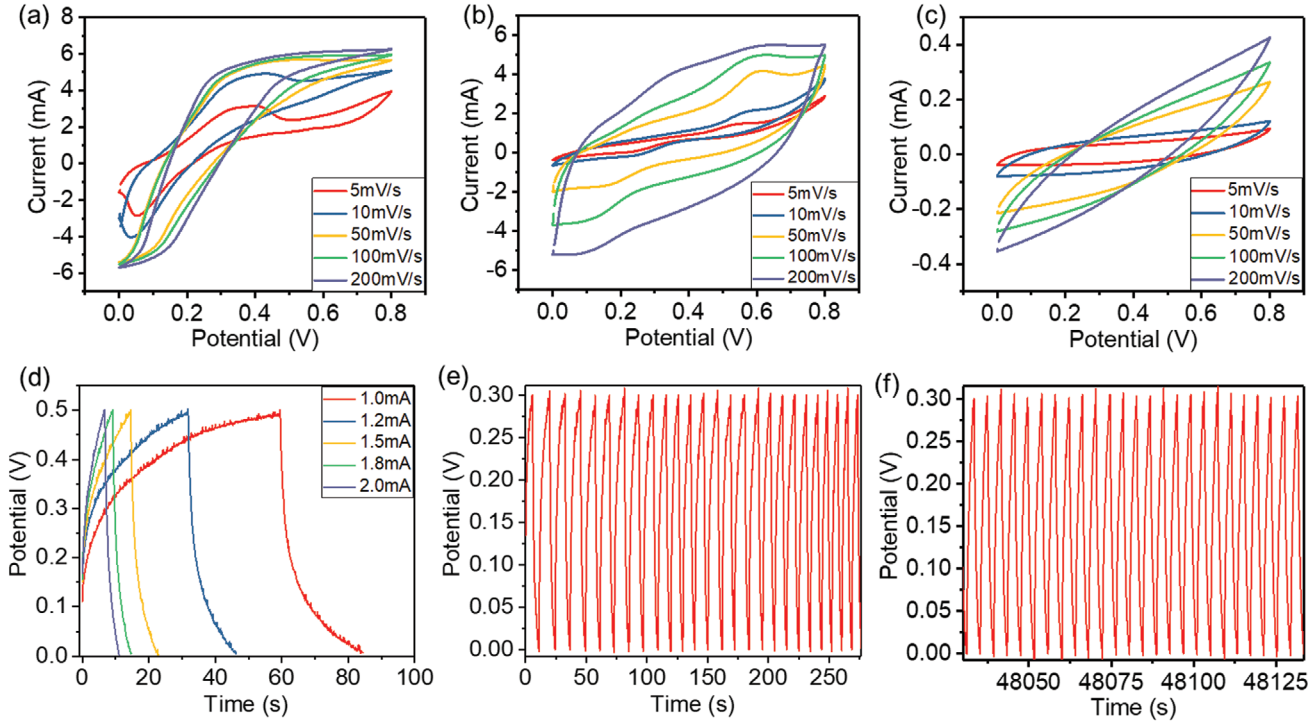

Figure 6. a–c) CV curves of AFR-Gr, ND-Gr, and CP-Gr based SCs, respectively, d) GCD curves of ND-Gr based SC at different currents. e) First 25 cycle and f) last 25 cycle of 5000 GCD cycles of ND-Gr based SC (in PVA-KCl gel electrolyte).

GCD curve of AFR-Gr based SC with different applied current was given in Figure S8 in the Supporting Information.

Stability of the device performance against mechanical deformation is a prime consideration for wearable applications. Hence, we have evaluated the capacitance retention of AFR-Gr and ND-Gr based FSCs with different bending radii. **Figure 7**a shows a good capacitance retention (above 90%) for all bending radii, suggesting the mechanical stability of the fabricated FSCs. As a proof of concept, we have powered a textile based wearable temperature sensor[24] with the fabricated FSCs. Figure 7b shows the sensor output (from room temperature to 80 °C) by powering with FSCs and it shows a linear response with a high sensitivity of −133 Ω °C^{-1}. Figure 7c depicts the long-term stability of sensor powered by FSC at room temperature, indicating the uniform power delivery from the SC. Figure 7d demonstrates a prototype of wearable wristband contains FSCs integrated temperature sensor for real time monitoring. Apart from this, we were also able to power a 1.6 V light-emitting diode (LED) (Figure S9, Supporting Information) with an array of FSCs. All these results imply the practical suitability of the fabricated devices for wearable applications.

2.3. Comparison of Graphite Printed Textile Based SCs Performance

As this study is a foundational study for the development of nontoxic wearable FSCs, we have also analyzed the performance of the fabricated device in acidic and alkaline gel electrolyte. **Figure 8** compares the performance of graphite coated fabric based SCs with different conducting fabrics as current collectors and different electrolytes. Figure 8a,b compare C_A and energy density and Figure 8c shows the Ragone plot of different fabrics with KCl-PVA gel electrolyte. It is evident from Figure 8a that the maximum C_A for AFR-Gr was 99.06 mF cm^{-2}. A similar trend is witnessed for the energy density. In comparison with all the devices under study, the AFR-Gr had the highest energy density of 8.81 μWh cm^{-2} (Figure 8b). It is also interesting to note that the introduction of graphite on the conducting metal fabric significantly enhanced the properties of the SC. In the case of Nora Dell fabric-based SC, the C_A was approximately four times greater when it is coated with graphite. Likewise, it was doubled in the case of Armor FR. A similar observation was found for the energy density of both devices. In comparison with the metal-free graphite coated FSC (CP-Gr), the metal coated FSCs have six times (ND) and 26 times (AFR) greater C_A. This was further enhanced by 24 times (ND-Gr) and 52 times (AFR-Gr) when the graphite paste was applied to the metal coated fabric devices. This enhancement in performance for FSC 3 as compared to FSC 1 and FSC 2 could be due to the involvement of both Faradaic and EDLC capacitance. From the Ragone plot (Figure 8c), it can be noticed that the bare Nora Dell based SC shows the highest power density and AFR-Gr gives the highest energy density from all fabricated devices with KCl-PVA solid electrolyte. A detailed comparison of both areal and mass specific capacitance, energy and power densities of AFR-Gr and ND-Gr in PVA-KCl gel electrolyte was given in Table S2 in the Supporting Information. Similar to this investigation, the Figure 8d–f shows the performance analysis of ND-Gr and AFR-Gr devices in different gel electrolytes such as acidic (PVA-H_3PO_4), alkaline (PVA-NaOH), and neutral

© 2020 The Authors. Published by WILEY-VCH Verlag GmbH & Co. KGaA, Weinheim

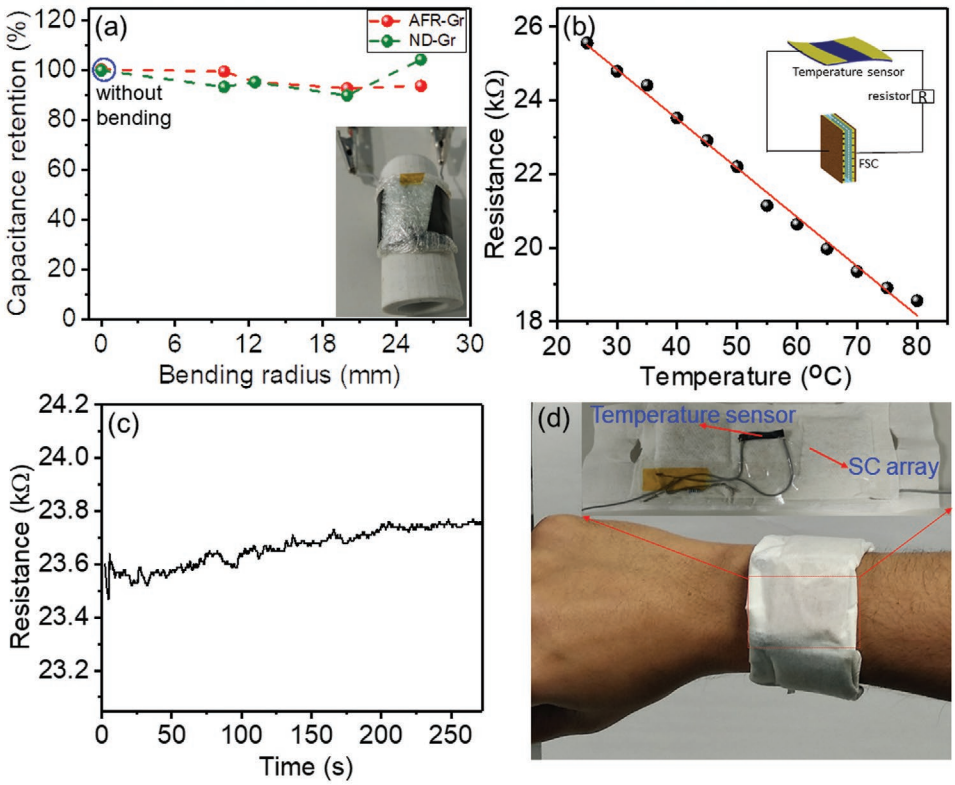

Figure 7. a) Capacitance retention of AFR-Gr and ND-Gr based SCs at different bending radii (Inset figure shows that the FSC fixed on 3D printed mount with radius of curvature 12.5 mm), b) resistance variation with temperature of wearable temperature sensor powered by FSCs (Inset shows the circuit used), c) resistance variation of temperature sensor at 25 °C with time under constant power supply from FSCs, and d) photographs of FSC based wearable power band for temperature sensor (inset shows the assembly of sensor with FSC).

(PVA-KCl). It is obvious from Figure 8d that for both devices the maximum specific capacitance and energy density are obtained with PVA-H_3PO_4 gel electrolyte. AFR-Gr device shows a C_A value of 213 mF cm^{-2}, which is the highest value achieved among all the devices used in this investigation. This is rationalized by the small ionic radius of H^+ ion in H_3PO_4-PVA gel electrolyte, which eases the diffusion of cations through the graphite electrode, which in turn results in a high capacitance.[25] Similar is the case with energy density variation also. However, for wearable applications the neutral electrolyte based SCs are preferred as any toxicity due to electrolyte leakage is unacceptable. Hence, in the present study we selected the PVA-KCl based SC as a wearable energy storage device. The C_A value of the Armor FR based SC is compared with reported textile based SCs. The results show an enhanced performance in comparison with some of the previously reported works (shown in Table 1). As a future objective, this FSC can be used to deliver power for flexible electronic system which require small amount of power,[26] and the performance of the device may be improved by using liquid metal (have more flexibility and stretchability) for wearable application.[27]

2.4. Cytocompatibility of PVA-KCl Gel Electrolyte

The biocompatibility of wearable technologies is a crucial parameter that must be assessed to ensure that innovative devices perform adequately without inducing adverse bodily reactions. As per the International Standard testing method International Organization for Standardization (ISO) 10993-5, the first step toward determining the biocompatibility of a device is the examination of device cytocompatibility (ISO 10993-1:2018). In the current study, the cytocompatibility of the PVA-KCl gel electrolyte was assessed by observing the adhesion and proliferation of HDFa cells on the electrolyte surface.[28] HDFas seeded on the untreated wells of the cell culture dishes began to attach after 3 h. As depicted in **Figure 9**, the untreated cells exhibited a flat morphology and were well spread throughout the well of the culture dish. In contrast, HDFas seeded on the surface of the PVA-KCl gel electrolyte remained round and showed little attachment. Although proliferation continued, the rate of growth slowed in comparison to cells seeded within the untreated culture wells, as can be observed in Figure 9. Considering that the cell death was not induced in the presence of the PVA-KCl gel electrolytes and growth was not inhibited, the current findings suggest that the gel electrolytes are not toxic to HDFas but are also not suitable scaffolds to enhance prolific growth. This is likely due to the extremely hydrophilic nature of PVA which has previously been reported to prevent cell adhesion.[29]

3. Conclusion

We have successfully validated the use of commercial metal coated fabrics as a current collector and electrode material

© 2020 The Authors. Published by WILEY-VCH Verlag GmbH & Co. KGaA, Weinheim

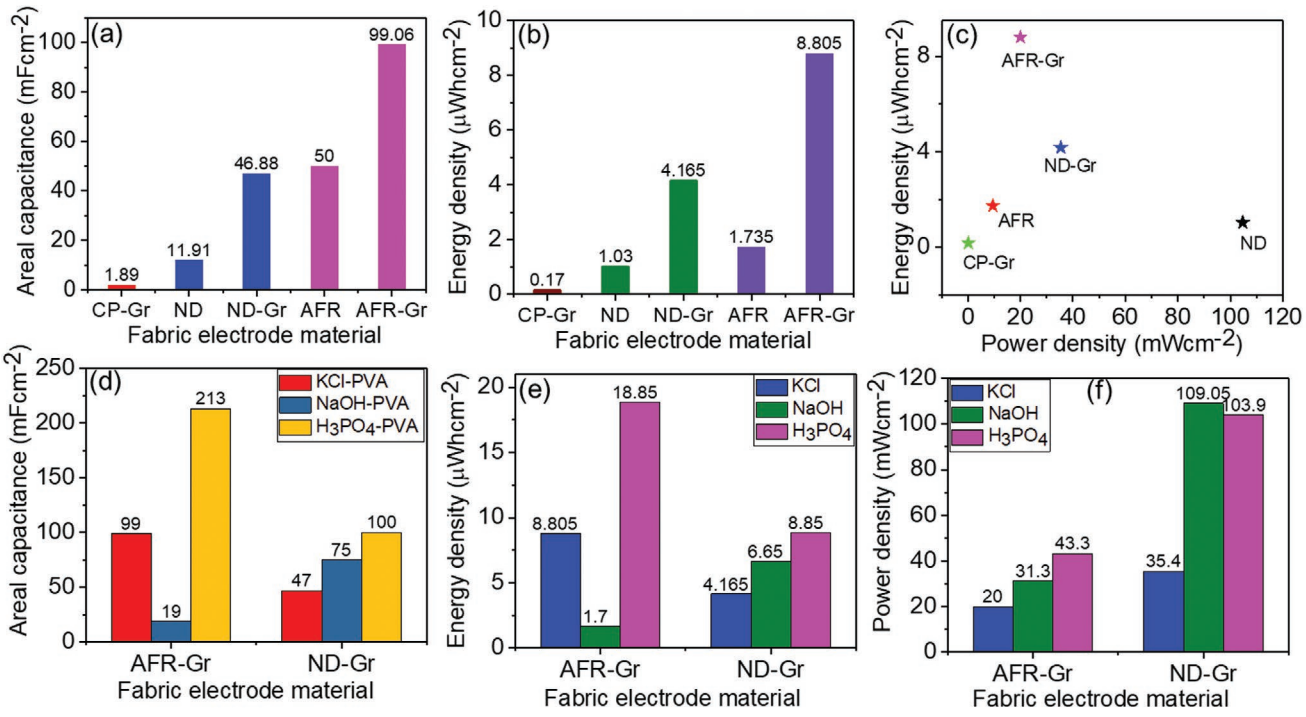

Figure 8. Comparison of a) areal capacitance, b) energy density, and c) ragone plot of different SCs with PVA-KCl gel electrolyte, and d) areal capacitance, e) energy density, and f) power density of different SC with different gel electrolyte.

for wearable SC applications. The role of different electrolyte as well as the influence of concentration of KCl electrolyte on the performance of the SC devices was investigated. The comparison of graphite coated SC with metal coated textiles indicates a high enhancement in the performance of metal coated fabric-based SC. In this work, both AFR-Gr and ND-Gr electrode and PVA-KCl electrolyte based SCs demonstrated good performance. Among this, the AFR-Gr based SC in PVA-H_3PO_4 gives the maximum C_A (213 mF cm^{-2}) and energy density (18.85 μWh cm^{-2}). The ND-Gr based SC exhibited a C_A of 46.88 mF cm^{-2}, energy density of 4.17 μWh cm^{-2}, and power density of 35.4 mW cm^{-2}, with a good cyclic stability of 5000 GCD cycles. It is also noted that the metal coated FSC without graphite electrode gives high performance (C_A of 11.91 mF cm^{-2} for Nora Dell and 50 mF cm^{-2} for Armor FR) compared to that of graphite coated bare cellulose-polyester based SC (1.89 mF cm^{-2}). All these results suggest that metal coated fabrics are suitable candidates for wearable SC applications, compared to carbon (graphite) coated FSC. The biocompatibility test by observing the adhesion and proliferation of HDFa cells on the electrolyte surface shows the nontoxicity nature of the PVA-KCl gel electrolyte in wearable SC.

4. Experimental Section

Materials: In this work, SCs were fabricated by using 1) commercial conductive fabrics and 2) a conductive fabric developed using graphite paste. Four different types of commercial conductive fabrics were used namely i) Berlin RS, ii) Bremen RS, iii) Nora Dell from Statex Produktions-und Vertriebs GmbH, Germany, and iv) Armor FR from V Technical textiles Inc. US. These fabrics functioned as both an electrode

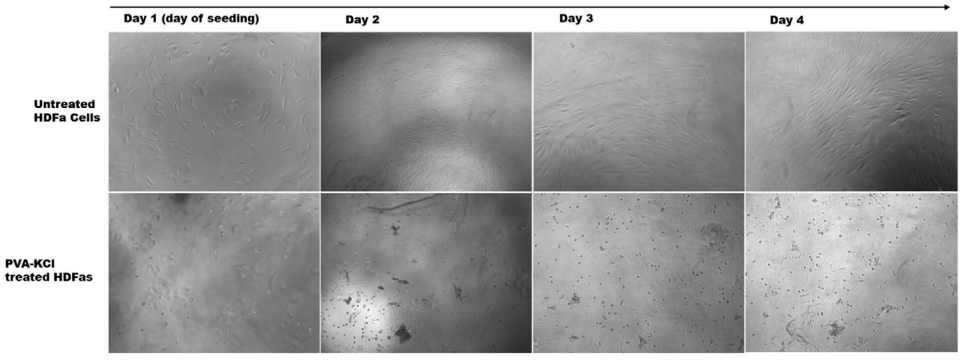

Figure 9. Optical microscopy images of untreated HDFas and those treated with PVA-KCl gel electrolytes for wearable applications.

© 2020 The Authors. Published by WILEY-VCH Verlag GmbH & Co. KGaA, Weinheim

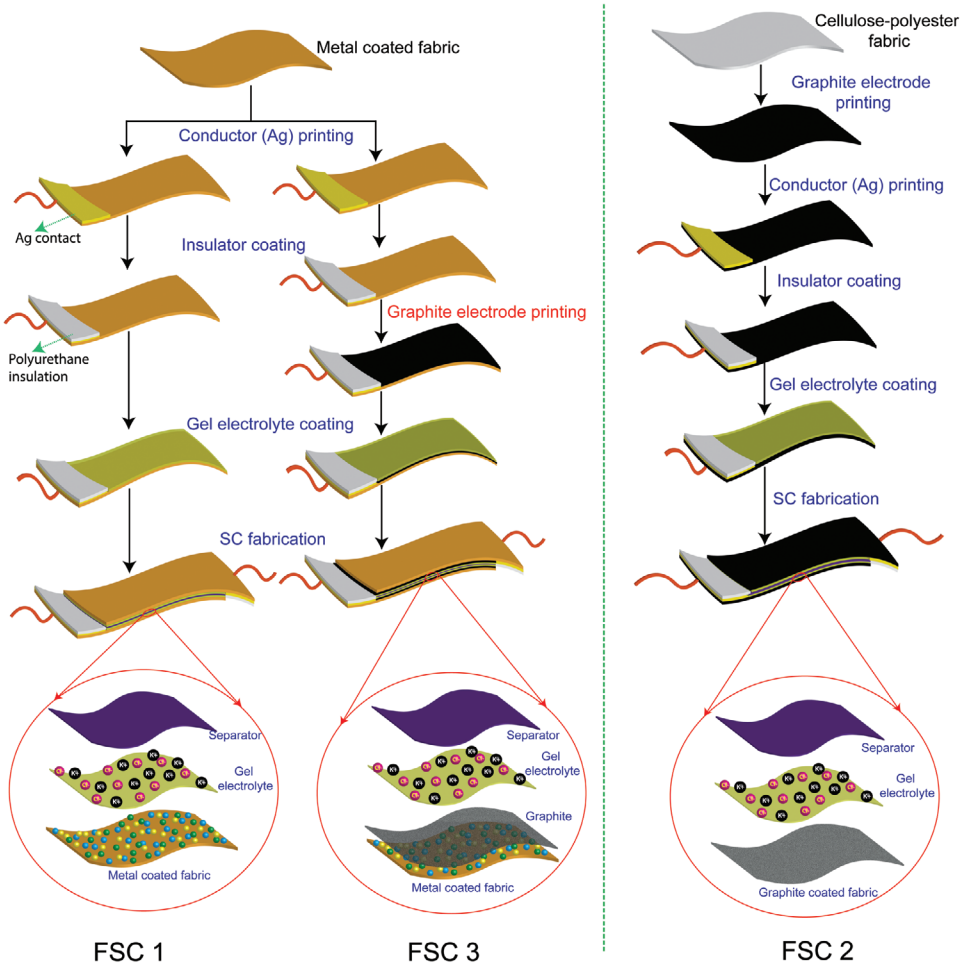

Figure 10. Schematics of textile based SCs fabrication.

and a current collecting material for the FSC. A metal free bare fabric of cellulose-polyester (Techni Cloth, TX 612) was also used for the graphite coated SC fabrication to compare the performance with metal deposited fabric SCs. Graphite Paste (35%) was prepared in terpineol (Sigma-Aldrich) solvent, using Triton X-100 (3%, Sigma-Aldrich) as a dispersant and ethyl cellulose (10%, Sigma-Aldrich) as the binder by mixing at room temperature through magnetic stirring for 6 h. The prepared paste was printed on top of the cellulose/polyester cloth and on the top of metal coated cloth.

SC Fabrication: Three types of FSC were fabricated; i) FSC 1, where the electrode material was based on a metal coated conducting fabric, ii) In FSC 2 the electrode is composed of graphite paste printed on top of a nonconductive polyester/cellulose cloth, and iii) FSC 3, in which the electrode was composed of graphite paste printed on top of metal coated conducting fabric used for FSC 1. In all FSCs the total electrode area is 4 cm^2. The schematic representation, comparing the fabrication of FSCs, is shown in **Figure 10**. A silver wire was used for external connection and it was fixed on top of the conducting fabric using silver (Ag) conductive epoxy (from RS components, 186-3600). A polyester/cellulose blend (Techni Cloth, TX 612) was used as a separator and polyurethane based resin as an insulating layer.[14a,30] In the case of graphite coated FSC fabrication the formulated graphite paste was printed on the fabric (both metalized and unmetallized), dried at 75 °C in a hot air oven for 2 h, and used as a flexible electrode. The influence of electrolytes such as KCl, H_3PO_4, and NaOH was also investigated on the performance of the SCs. The aqueous KCl electrolyte was prepared by dissolving different amounts of KCl salt in water (0.1. 0.5, 1.0, and 2.0 M electrolyte solutions). For the gel electrolytes, first the 1 g of PVA was dissolved in 10 mL of water under heating at 85 °C for 1 h followed by the addition of the KCl solution dissolved in water. A similar procedure was adopted for the preparation of H_3PO_4 and NaOH based gel electrolyte also. The mass fraction of KCl, H_3PO_4, and NaOH in the final gel (with respect to PVA) was around 0.67, 0.79, and 0.5, respectively.

Characterizations: The structural and phase analysis of the metal coated fabrics, before and after electrochemical reactions, were carried out using XRD (P'Analytical X'Pert with Cu K_α (λ = 1.541 Å), SEM (Hitachi SU8240), and EDX (Hitachi SU8240 EDX). The viscosity of the formulated paste was measured by rotational viscometer (VCPL 450015, Cole-Parmer). The electrochemical analysis including CV and EIS was measured using an electrochemical workstation (Metrohm Autolab, PGSTAT302N), with a two electrodes system. The CV studies were carried out at scan rates ranging between 1 and 200 mV s^{-1} in a potential range between 0 and 0.8 V. The EIS analysis was carried out by applying an alternating-current signal in the frequency range of 1 mHz to 1 MHz in a potential amplitude of 10 mV. The capacitance (C), areal capacitance (C_A), energy density (E_A), and power density (P_A) were calculated from the CV and EIS analysis by using the following equations

$$C_A = \frac{\int I dV}{2A\Delta V v} \quad (4)$$

$$E_A = 0.5 C_A (\Delta V)^2 \quad (5)$$

$$P_A = \frac{(\Delta V)^2}{4AESR} \quad (6)$$

© 2020 The Authors. Published by WILEY-VCH Verlag GmbH & Co. KGaA, Weinheim

where $\int Id\nu$ is the area under the CV curve, ΔV is the operating potential window (V), ν is the scan rate (V s^{-1}), A is area (cm^2), and ESR is the equivalent series resistance (Ω). The galvanostatic charging–discharging (GCD) measurements were made by using source meter (Agilent, U2722A) controlled with LabVIEW program at different current densities.

Bending Analysis and Wearable Applications: The static bending test of FSCs was carried out by CV analysis of the SC wrapped on top of semicylinders having radii of 10, 12.5, 20, and 26 mm, respectively.[14a] As a proof of concept for demonstrating the practical application of the FSCs, a wearable temperature sensor (made of pristine poly (3,4-ethylenedioxythiophene): poly(styrenesulfonate) (PEDOT: PSS) coated fabrics) was powered. The fabrication steps of the temperature sensor were reported in the previous work.[24,31] The textile-based sensor was kept on a hot plate and varied the temperature in the range of 25–80 °C. The charged SC was used to operate (applied ≈200 mV) the sensors through load resistance (the electronic circuit for operating the sensor was similar to the previous work[1b]) and the observed variation in resistance with temperature was monitored.

Biocompatibility Studies—Cell Culture: HDFa cells were used to assess the in vitro cytocompatibility of the PVA-KCl gel electrolyte. HDFa cells, obtained from Thermo Fisher Scientific, were cultured at log phase growth in standard culture conditions (37 °C in a 5% CO_2 incubator on tissue culture dishes) using Medium 106 (fibroblasts) complemented with a Low Serum Growth supplement containing fetal bovine serum, basic fibroblast growth factor, heparin, hydrocortisone, and an epidermal growth factor (Thermo Fisher). Cells were dissociated using 1× trypsin/ethylenediaminetetraacetic acid solution (Thermo Fisher) for 1–3 min at room temperature, followed by serum inactivation. Cells were counted using a hemocytometer, collected by centrifugation and resuspended in growth media at a density of 1×10^4 cells mL^{-1}.

Biocompatibility Studies—Cytocompatibility Testing: Prior to cell exposure, the PVA-KCl gel electrolyte was sterilized with ethanol and extensively washed with sterile phosphate buffered saline solution. The electrolyte was then aseptically transferred to individual wells of a 96-well cell culture plate. 100 µL of the 1×10^4 HDFa cell suspension was seeded on top of the PVA based gel electrolytes. After incubation (37 °C in a 5% CO_2 incubator on tissue culture dishes), the morphology of cells surrounding the PVA-KCl gel electrolyte was observed using an optical microscope every 24, 48, and 72 h.

The experiment involving human subject has been performed with the full, informed consent of the volunteer.

Supporting Information

Supporting Information is available from the Wiley Online Library or from the author.

Acknowledgements

This work was supported in part by the Royal Society and the Science and Engineering Research Board of India (SERB) through Newton International Fellowship (NIF\R1\182437), Engineering and Physical Sciences Research Council through Engineering Fellowship for Growth (EP/M002527/1 and EP/R029644/1), and European Commission through Aquasense project (H2020-MSCA-ITN-2018-813680). The authors are thankful to James Watt Nanofabrication Centre (JWNC) and Electronic Systems Design Centre (ESDC) at University of Glasgow for support related to fabrication and characterization.

Conflict of Interest

The authors declare no conflict of interest.

Keywords

biocompatibility, fabric supercapacitors, gel electrolytes, graphite, metal nanoparticles

Received: December 12, 2019
Revised: February 9, 2020
Published online: February 28, 2020

[1] a) G. Qu, J. Cheng, X. Li, D. Yuan, P. Chen, X. Chen, B. Wang, H. Peng, *Adv. Mater.* **2016**, *28*, 3646; b) L. Manjakkal, C. G. Núñez, W. Dang, R. Dahiya, *Nano Energy* **2018**, *51*, 604; c) K. Jost, G. Dion, Y. Gogotsi, *J. Mater. Chem. A* **2014**, *2*, 10776; d) R. Dahiya, *Proc. IEEE* **2019**, *107*, 247; e) C. G. Núñez, W. T. Navaraj, E. O. Polat, R. Dahiya, *Adv. Funct. Mater.* **2017**, *27*, 1606287; f) C. García Núñez, L. Manjakkal, R. Dahiya, *npj Flexible Electron.* **2019**, *3*, 1; g) R. Dahiya, N. Yogeswaran, F. Liu, L. Manjakkal, E. Burdet, V. Hayward, H. Jörntell, *Proc. IEEE* **2019**, *107*, 2016.

[2] a) S. Lei, Y. Liu, L. Fei, R. Song, W. Lu, L. Shu, C. L. Mak, Y. Wang, H. Huang, *J. Mater. Chem. A* **2016**, *4*, 14781; b) L. Manjakkal, A. Pullanchiyodan, N. Yogeswaran, E. Hosseini, R. Dahiya, *Adv. Mater.* **2020**, in press, https://doi.org/10.1002/adma.201907254.

[3] X. Pu, L. Li, M. Liu, C. Jiang, C. Du, Z. Zhao, W. Hu, Z. L. Wang, *Adv. Mater.* **2016**, *28*, 98.

[4] a) J. H. Kim, C. Choi, J. M. Lee, M. J. de Andrade, R. H. Baughman, S. J. Kim, *Sci. Rep.* **2018**, *8*, 13309; b) L. Liu, Y. Yu, C. Yan, K. Li, Z. Zheng, *Nat. Commun.* **2015**, *6*, 7260; c) A. Rafique, A. Massa, M. Fontana, S. Bianco, A. Chiodoni, C. F. Pirri, S. Hernandez, A. Lamberti, *ACS Appl. Mater. Interfaces* **2017**, *9*, 28386; d) M. Hu, T. Hu, R. Cheng, J. Yang, C. Cui, C. Zhang, X. Wang, *J. Energy Chem.* **2018**, *27*, 161.

[5] L. Manjakkal, W. Dang, N. Yogeswaran, R. Dahiya, *Biosensors* **2019**, *9*, 14.

[6] S. Zhai, H. E. Karahan, L. Wei, Q. Qian, A. T. Harris, A. I. Minett, S. Ramakrishna, A. K. Ng, Y. Chen, *Energy Storage Mater.* **2016**, *3*, 123.

[7] a) M. Pasta, F. La Mantia, L. Hu, H. D. Deshazer, Y. Cui, *Nano Res.* **2010**, *3*, 452; b) L. Bao, X. Li, *Adv. Mater.* **2012**, *24*, 3246; c) L. Bao, J. Zang, X. Li, *Nano Lett.* **2011**, *11*, 1215; d) L. Hu, W. Chen, X. Xie, N. Liu, Y. Yang, H. Wu, Y. Yao, M. Pasta, H. N. Alshareef, Y. Cui, *ACS Nano* **2011**, *5*, 8904; e) Z. Gui, H. Zhu, E. Gillette, X. Han, G. W. Rubloff, L. Hu, S. B. Lee, *ACS Nano* **2013**, *7*, 6037; f) T. G. Yun, B. i. Hwang, D. Kim, S. Hyun, S. M. Han, *ACS Appl. Mater. Interfaces* **2015**, *7*, 9228; g) Q. Xue, J. Sun, Y. Huang, M. Zhu, Z. Pei, H. Li, Y. Wang, N. Li, H. Zhang, C. Zhi, *Small* **2017**, *13*, 1701827.

[8] a) J. E. Yoo, J. Bae, *Macromol. Res.* **2015**, *23*, 749; b) G. Nagaraju, Y. H. Ko, J. S. Yu, *CrystEngComm* **2014**, *16*, 11027; c) W. C. Li, C. L. Mak, C. W. Kan, C. Y. Hui, *RSC Adv.* **2014**, *4*, 64890.

[9] S. Wen, J.-W. Lee, I.-H. Yeo, J. Park, S.-i. Mho, *Electrochim. Acta* **2004**, *50*, 849.

[10] a) L. Hu, M. Pasta, F. La Mantia, L. Cui, S. Jeong, H. D. Deshazer, J. W. Choi, S. M. Han, Y. Cui, *Nano Lett.* **2010**, *10*, 708; b) K. Jost, C. R. Perez, J. K. McDonough, V. Presser, M. Heon, G. Dion, Y. Gogotsi, *Energy Environ. Sci.* **2011**, *4*, 5060; c) K. Song, X. Wang, J. Wang, B. Zhang, R. Yang, *ChemistrySelect* **2019**, *4*, 1685.

[11] a) I. Shakir, Z. Ali, J. Bae, J. Park, D. J. Kang, *Nanoscale* **2014**, *6*, 4125; b) Y. Yang, Q. Huang, L. Niu, D. Wang, C. Yan, Y. She, Z. Zheng, *Adv. Mater.* **2017**, *29*, 1606679.

[12] I. Shakir, Z. Ali, J. Bae, J. Park, D. J. Kang, *RSC Adv.* **2014**, *4*, 6324.

[13] W. C. Li, C. L. Mak, C. W. Kan, C. Y. Hui, *RSC Adv.* **2014**, *4*, 64890.

[14] a) L. Manjakkal, W. T. Navaraj, C. G. Núñez, R. Dahiya, *Adv. Sci.* **2019**, *6*, 1802251; b) M. A. Kafi, A. Paul, A. Vilouras, R. Dahiya, *Biosens. Bioelectron.* **2020**, *147*, 111781.

© 2020 The Authors. Published by WILEY-VCH Verlag GmbH & Co. KGaA, Weinheim

[15] N. T. Trang, H. V. Ngoc, N. Lingappan, D. J. Kang, *Nanoscale* **2014**, *6*, 2434.
[16] L. Manjakkal, D. Shakthivel, R. Dahiya, *Adv. Mater. Technol.* **2018**, *3*, 1800252.
[17] B.-A. Mei, O. Munteshari, J. Lau, B. Dunn, L. Pilon, *J. Phys. Chem. C* **2018**, *122*, 194.
[18] L. Manjakkal, E. Djurdjic, K. Cvejin, J. Kulawik, K. Zaraska, D. Szwagierczak, *Electrochim. Acta* **2015**, *168*, 246.
[19] a) M. J. Siegfried, K.-S. Choi, *Angew. Chem., Int. Ed.* **2008**, *47*, 368; b) T. Nguyen, M. d. F. Montemor, *Adv. Sci.* **2019**, *6*, 1801797; c) A. I. Inamdar, Y. Kim, S. M. Pawar, J. H. Kim, H. Im, H. Kim, *J. Power Sources* **2011**, *196*, 2393.
[20] W.-w. Liu, X.-b. Yan, J.-w. Lang, C. Peng, Q.-j. Xue, *J. Mater. Chem.* **2012**, *22*, 17245.
[21] A. Borenstein, O. Hanna, R. Attias, S. Luski, T. Brousse, D. Aurbach, *J. Mater. Chem. A* **2017**, *5*, 12653.
[22] S. Lehtimaki, A. Railanmaa, J. Keskinen, M. Kujala, S. Tuukkanen, D. Lupo, *Sci. Rep.* **2017**, *7*, 46001.
[23] J. Zhu, Y. Xu, J. Wang, J. Lin, X. Sun, S. Mao, *Phys. Chem. Chem. Phys.* **2015**, *17*, 28666.
[24] L. Manjakkal, M. Soni, N. Yogeswaran, R. Dahiya, presented at 2019 *IEEE Int. Conf. Flexible Printable Sens. Syst. (FLEPS)*, Glasgow, July **2019**.
[25] Q. Chen, X. Li, X. Zang, Y. Cao, Y. He, P. Li, K. Wang, J. Wei, D. Wu, H. Zhu, *RSC Adv.* **2014**, *4*, 36253.
[26] M. J. Christoe, J. Han, K. Kalantar-Zadeh, *Adv. Mater. Technol.* **2020**, *5*, 1900733.
[27] J. Yang, W. Cheng, K. Kalantar-zadeh, *Proc. IEEE* **2019**, *107*, 2168.
[28] M. A. Kafi, K. Aktar, M. Todo, R. Dahiya, *Regener. Biomater.* **2019**, 1, https://doi.org/10.1093/rb/rbz034.
[29] a) Y. Wu, C. Yu, M. Xing, L. Wang, G. Guan, *J. Biomed. Mater. Res. B* **2020**, *108*, 117; b) T. Gao, M. Jiang, X. Liu, G. You, W. Wang, Z. Sun, A. Ma, J. Chen, *Polymers (Basel, Switz.)* **2019**, *11*, 171; c) T. Miao, E. J. Miller, C. McKenzie, R. A. Oldinski, *J. Mater. Chem. B* **2015**, *3*, 9242.
[30] L. Manjakkal, A. Vilouras, R. Dahiya, *IEEE Sens. J.* **2018**, *18*, 7779.
[31] M. Soni, M. Bhattacharjee, M. Ntagios, R. Dahiya, *IEEE Sens. J.* **2020**, *99*, 1.

© 2020 The Authors. Published by WILEY-VCH Verlag GmbH & Co. KGaA, Weinheim